Smart Structures and Systems, *Vol. 30, No. 1 (2022) 107-119*
https://doi.org/10.12989/sss.2022.30.1.107

Modal identification of time-varying vehicle-bridge system using a single sensor

Yilin Li [1a], Wen-Yu He*[1,2], Wei-Xin Ren [3b], Zhiwei Chen [4c] and Junfei Li [1d]

[1] *Department of Civil Engineering, Hefei University of Technology, Hefei, Anhui 230009, China*
[2] *Anhui Engineering Laboratory for Infrastructural Safety Inspection and Monitoring, Hefei University of Technology, Hefei, Anhui 230009, China*
[3] *College of Civil and Transportation Engineering, Shenzhen University, Shenzhen, Guangdong 518061, China*
[4] *Department of Civil Engineering, Xiamen University, Xiamen, 361005, China*

(*Received November 16, 2021, Revised March 2, 2022, Accepted April 11, 2022*)

Abstract. Modal parameters are widely used in bridge damage detection, finite element model (FEM) updating and design optimization. However, the conventional modal identification approaches require large number of sensors, enormous data processing workload, but normally result in mode shapes with low accuracy. This paper proposes a modal identification method of time-varying vehicle-bridge system using a single sensor. Firstly, the essential physical relationship between the instantaneous frequency of the vehicle-bridge system and the bridge mode shapes are derived. Subsequently, based on the synchroextracting transform, the instantaneous frequency of the system is tracked through the dynamic response collected by a single sensor, and further the modal parameters are estimated by using the derived physical relationship. Then numerical and experimental examples are conducted to examine the feasibility and effectiveness of the proposed method. Finally, the modal parameters identified by the proposed method are applied in bridge FEM updating. The results manifest that the proposed method identifies the modal parameters with high accuracy via a single sensor, and can provide reliable data for the FEM updating.

Keywords: modal parameters; moving vehicle-bridge system; synchroextracting transform; time-frequency analysis; time-varying

1. Introduction

Bridge modal parameters including frequency, mode shape and damping ratio are widely used in bridge damage detection, finite element model (FEM) updating and design optimization (Zhang *et al*. 2019, Chang *et al*. 2019, Ribeiroa *et al*. 2012). Therefore, increasing attention has been paid to modal identification techniques in the field of bridge engineering (Obrien and Malekjafarian 2016, Babakhani *et al*. 2018, Mahato *et al*. 2020). Traditional methods utilize a large number of sensors to measure the structural dynamic responses, and followed by complex signal processing tools to obtain the modal parameters (Zhang *et al*. 2022). Though such methods have been studied and applied extensively, two shortcomings are gradually emerging and should not be ignored: (a) To obtain high spatial resolution mode shapes, a large number of sensors are required to be arranged densely, or multiple test setups should be implemented, which would not only increase the workload and difficulties in modal testing but also the computation amount in the following modal analysis; (b) Compared to natural frequency, mode shape identification has obvious difficulties in the aspects of the complexity of signal processing technique and the identification accuracy. Thus, developing identification methods in which only a small number of sensors are required becomes the urgent demand. Yang *et al*. (Yang *et al*. 2004, Yang and Lin 2005) proposed an indirect method to extract bridge frequencies by installing one sensor on the moving vehicle and verified it via numerical simulation. Yang *et al*. (2012) constructed the bridge mode shapes by applying the Hilbert Transform on the vehicle response collected by a single sensor. Besides, the influence of moving velocity and road surface roughness on construction accuracy was investigated systematically. Further González *et al*. (2012) installed one sensor on the dual-degree-of-freedom vehicle model to identify the bridge damping. The effects of various factors such as bridge span, vehicle velocity, road surface roughness and measurement noise on the identification accuracy were studied through numerical simulations. Kong *et al*. (2016) proposed a bridge frequency and mode shape extraction approach based on the response collected by a single sensor installed in an experimental vehicle model composed of a trailer (traction vehicle) and two trailers.

The mass of the vehicle is assumed to be much less than the bridge mass for simple in the above-mentioned studies. However, the modal parameters of the vehicle-bridge system (VBS) are found to be different from the modal

*Corresponding author, Ph.D., Professor,
E-mail: wyhe@hfut.edu.cn
[a] Ph.D. Student
[b] Ph.D., Professor
[c] Ph.D., Professor
[d] Ph.D. Student

ISSN: 1738-1584 (Print), 1738-1991 (Online)

parameters of bridge when the mass ratio of the vehicle to the bridge cannot be ignored (Magrab 2012). Frýba (1996) stated that the frequency of the VBS was different from the frequency of the bridge itself by simulating the train as a uniform mass. Kim *et al*. (2003) found that the frequency of the stationary VBS was reduced by 5.4% compared with the natural frequency of the bridge through field experiments. Yang *et al*. (2013) simulated the vehicle as a single-degree-of-freedom sprung mass model, and derived the closed solution of the frequencies for the VBS by considering only the first mode. The influences of factors such as different axle mass ratio and natural frequency ratio on the system frequency were discussed. Xin *et al*. (2019) proposed an enhanced Empirical Wavelet Transform (EWT) approach based on Synchroextracting Transform (SET) for time-varying system identification. Ni *et al*. (2018) proposed a new time-varying system identification approach by using variational mode decomposition, which could identify the instantaneous frequencies with a better accuracy than the traditional methods. Considering the fact that the vehicle locates on different positions of the bridge, the characteristics of the VBS are notably time-varying. Though the time-varying frequency analysis has been studied extensively (Li *et al*. 2020, Zhang *et al*. 2021), relatively few attentions have been paid on the mode shape extraction. He *et al*. (2018) deduced the essential physical relationship between the frequency variation of the single-point additional mass-bridge system and the amplitude of the bridge mass-normalized mode shape at the contact position. Further a bridge mode shape identification technique was proposed based on the frequencies of the parked VBSs accordingly. The main advantage of this technique was that it could avoid the disadvantages of expensive and inconvenient installation of measuring equipment on site, and does not need to increase the number of sensors to improve the spatial resolution of the mode shapes. However, the identification process was time-consuming as the test vehicle should be parked at different positions gradually. This paper proposes a modal identification method of time-varying VBS. A single sensor is installed on the bridge to collect the dynamic response of the moving VBS, and the instantaneous frequency (IF) of the moving VBS is identified by synchroextracting transform. Further IF is used to estimate the modal parameters of the bridge. Numerical examples and laboratory experiments are conducted to verify the effectiveness of the proposed method.

2. Basic theory

determined by the stiffness, mass and their distribution. As for the moving VBS, the mass distribution changes when the vehicle travels to different positions of the bridge (Kim and Kawatani 2008). Fig. 1 shows a typical VBS system in which the vehicle is simplified as a mass m_v supported by a spring of stiffness k_v. The parameters L,EI, ρ and A denote the bridge length, elastic modulus, mass density and cross section, respectively. The vehicle is assumed to move along the bridge deck at a constant velocity V. Supposing at time t, the vehicle moves to the

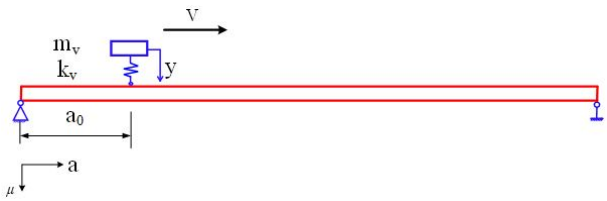

Fig. 1 The moving vehicle-bridge system

position with coordinate of a_0 along the beam axis a. The equation of motion of the moving VBS can be expressed as

$$p\ddot{\mu}(a,t) + EI\mu''''(a,t) = f_c(a,t)\delta(a-a_0) \tag{1}$$

$$m_v\ddot{z}(t) + k_v z(t) = k_v\mu(a_0,t) \tag{2}$$

$$a_0 = Vt \tag{3}$$

where $\mu(a,t)$ is the vertical displacement of the bridge, and δ is the Dirac delta function

The contact force between the vehicle and the bridge is

$$f_c = -m_v g - m_v\ddot{z}(t) \tag{4}$$

When the spring stiffness of the vehicle (k_v) is large enough, that is, $k_v \to \infty$, the vehicle displacement is

$$z(t) = \mu(a_0,t) \tag{5}$$

Thus, Eq. (4) is simplified as

$$f_c = -m_v g - m_v\ddot{\mu}(a_0,t) \tag{6}$$

Substituting Eq. (6) into Eq. (1)

$$\begin{aligned} &p\ddot{\mu}(a,t) + EI\mu''''(a,t) \\ &= [-m_v g - m_v\ddot{\mu}(a_0,t)]\delta(a-a_0) \end{aligned} \tag{7}$$

Based on the modal superposition, the vertical displacement of the beam can be written as

$$\mu(a,t) = \sum_{i=1}^{\infty} q_i(t)\varphi_i(a) \tag{8}$$

in which $\varphi_i(a)$ is the i^{th} mode shape of the bridge, and $q_i(t)$ is the corresponding modal coordinate.

Substituting Eq. (8) into Eq. (7), the motion equation of the bridge becomes

$$\begin{aligned} &p\sum_{i=1}^{\infty}\ddot{q}_i(t)\varphi_i(a) + EI\sum_{i=1}^{\infty} q_i(t)\varphi_i''''(a) \\ &= [-m_v g - m_v\sum_{i=1}^{\infty}\ddot{q}_i(t)\varphi_i(a_0)]\delta(a-a_0) \end{aligned} \tag{9}$$

Multiplying Eq. (9) by the bridge mass-normalized mode shape $\varphi_i(a_0)$ and integrated on $[0,L]$, the following equation can be obtained according to the orthogonality of the mass-normalized mode shape

$$\ddot{q}_i(t)[1+m_v\varphi_i^2(a_0)]+w_i^2q_i^2(t) = -m_v\varphi_i(a_0)\left[g+\sum_{n=1,n\neq i}^{\infty}\ddot{q}_i(t)\varphi_i(a_0)\right] \quad (10)$$

The natural frequency $w_i(a_0)$ of the VBS when the vehicle reaches the position a_0 is

$$w_i(a_0)=\sqrt{\frac{w_i^2}{1+m_v\varphi_i^2(a_0)}} \quad (11)$$

in which w_i is the i^{th} natural frequency of the bridge.

$$w_i=\frac{i^2\pi^2}{L^2}\sqrt{\frac{EI}{p}} \quad (12)$$

When the vehicle travels to position a_0, the relationship between the absolute value of the bridge mode shape amplitude and the vehicle induced frequency change can be expressed as

$$|\varphi_i(a_0)|=\sqrt{\frac{w_i^2-w_i^2(a_0)}{m_vw_i^2(a_0)}} \quad (13)$$

Eq. (13) clearly reveals the physical relationship between the VBS frequency, bridge frequency, vehicle mass and the amplitude of the bridge mode shape at position. It is the theoretical basis of the subsequent modal identification method. As the natural frequency of the VBS is time-varying, the system motion state at each sampling time point during the movement is deemed as stationary state for simplicity, thus the corresponding VBS frequency can be regarded as the IF at this sampling time point. And the mode shape identification can be transformed into frequency identification.

3. Modal identification method

3.1 Instantaneous frequency extraction

According to Eq. (13), the prerequisite for modal identification is extracting the IF of the moving VBS. Restricted by the Heisenberg uncertainty principle or unexpected cross terms, the traditional time-frequency analysis methods suffer from low time-frequency resolution, which leads to poor performance in characterizing the nonlinear behaviors of non-stationary signals. For example, synchrosqueezing transform squeezes the time-frequency coefficients into the IF trajectory only in the frequency direction, resulting in a lower time-frequency resolution (Oberlin *et al*. 2015, Yuan *et al*. 2021). The Wigner-Ville distribution can provide optimal energy concentration solutions for single-component linear FM signals, but unexpected cross terms occur when it is applied to nonlinear frequency modulated or multi-component signals (Boashash and Aïssa-El-Bey 2018). In view of this, Yu *et al*. (2017) proposed a time-frequency analysis method called synchroextracting transform (SET) inspired by the synchrosqueezing transform. The SET compresses all time-frequency coefficients into instantaneous frequency trajectories. Its main feature is retaining only the time-frequency information related to the time-varying features of the signal, and corresponding results allow signal reconstruction and mode decomposition. Thus, the SET is suitable for time-frequency analysis of multi-component signals with good robustness. This study combines the SET and short-time Fourier Transform (STFT) to estimate the IF of the moving VBS.

The STFT of a signal $s(t)$ with a real and even window $g(t)$ can be expressed as

$$S(t,\eta)=\int_{-\infty}^{+\infty}g(\varsigma-t)\cdot s(\varsigma)\cdot e^{-i\eta\varsigma}d\varsigma \quad (14)$$

in which $g(\varsigma-t)$ denotes the moving window, and $s(\varsigma)$ denotes the processed signal. The STFT expands a one-dimensional time-series signal into the two-dimensional time-frequency diagram for better observation effectiveness.

The STFT expression of $s(t)$ for a purely harmonic signal with frequency x_0 can be written as

$$S_q(t,\eta)=A\cdot\hat{g}(\eta-\eta_0)\cdot e^{i\eta_0t} \quad (15)$$

in which A is the invariant amplitude, and $\hat{g}(\eta-\eta_0)$ is the Fourier transform of the window function.

It is difficult to characterize the time-varying feature of a signal precisely. Therefore, the partial derivatives of Eq. (15) are calculated and sorted. The IF $\eta_0(t,\eta)$ of the signal on the two-dimensional time-frequency surface can be calculated as

$$\eta_0(t,\eta)=-i\cdot\frac{\partial_tS_q(t,\eta)}{S_q(t,\eta)} \quad (16)$$

in which $\Delta\eta$ is the discrete frequency interval.

As the response of the moving VBS is a non-stationary and multi-component signal, it can be expressed as

$$W_e(t,\eta)=\begin{cases}S_q(t,\eta)\ |\eta-\eta_0(t,\eta)|\le\dfrac{\Delta\eta}{2}\\ 0\ |\eta-\eta_0(t,\eta)|\ge\dfrac{\Delta\eta}{2}\end{cases} \quad (17)$$

in which $\Delta\eta$ is the discrete frequency interval.

As the response of the moving VBS is a non-stationary and multi-component signal, it can be expressed as

$$s(t)=\sum_{k=1}^{n}s_k(t)=\sum_{k=1}^{n}A_k(t)e^{i\psi_k(t)} \quad (18)$$

in which $\psi_k(t)$ and $\psi_k'(t)$ are the instantaneous phase and the IF of the k^{th} component, respectively. The STFT of $s(t)$ can be represented by the first-order approximation as Meignen *et al*. (2016)

$$S_q(t,\eta)\approx\sum_{k=1}^{n}A_k(t)\,\hat{g}(\eta-\eta_k'(t))e^{i\eta_k(t)} \quad (19)$$

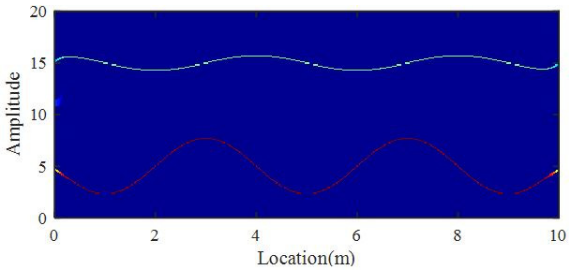

Fig. 2 The time-frequency diagram of the signal processed by the SET

For well-separated measured response, the IF of each mode can be estimated from

$$\psi'(t,\eta) = \sum_{k=1}^{n} \psi_k'(t,\eta) = -i \cdot \frac{\partial_t S_q(t,\eta)}{S_q(t,\eta)} \tag{20}$$

Considering the calculation error, the SET result can be re-written as

$$W_e(t,\eta) = \begin{cases} S_q(t,\eta) & |\eta - \psi'(t,\eta)| \le \dfrac{\Delta\eta}{2} \\ 0 & |\eta - \psi'(t,\eta)| \ge \dfrac{\Delta\eta}{2} \end{cases} \tag{21}$$

A multi-component signal S_1 expressed as Eq. (22) is considered as an example to illustrate the effectiveness of SET. Fig. 2 shows the time-frequency diagram of the signal S_1 processed by the SET. It can be seen that the energy of the identified time-frequency curve is highly concentrated, and the width of the time-frequency curve is narrow, which are meaningful in accurately extracting the time-frequency ridge.

$$\begin{aligned} S_1 = {} & 6 + 600sin[10\pi t + 11cos(0.5\pi t)] \\ & +300\cos[30\pi t + 3\sin(0.5\pi t)] \end{aligned} \tag{22}$$

3.2 Identification procedure

Modal identification procedure of the proposed method is shown in Fig. 3, details are as follows:

Step 1: Acceleration response collection. Install a single sensor on the bridge to collect the acceleration response of the moving VBS, and divide the response into two parts, i.e., the moving VBS dynamic response when the vehicle is running on the bridge and the bridge dynamic response after the vehicle running down the bridge.

Step 2: Bridge natural frequency identification. The dynamic response of the bridge after the vehicle running down the bridge is disposed by the FFT, and the result is deemed as Spectrogram 1. And the natural frequencies of the bridge are identified via peak-to-peak method.

Step 3: Acceleration response separation. The FFT is used to identify the spectrogram of the moving VBS dynamic response when the vehicle is running on the bridge, and the result is deemed as Spectrogram 2. Based on the result of bridge natural frequencies in Spectrogram 1, the band-pass filter is used to separate the acceleration

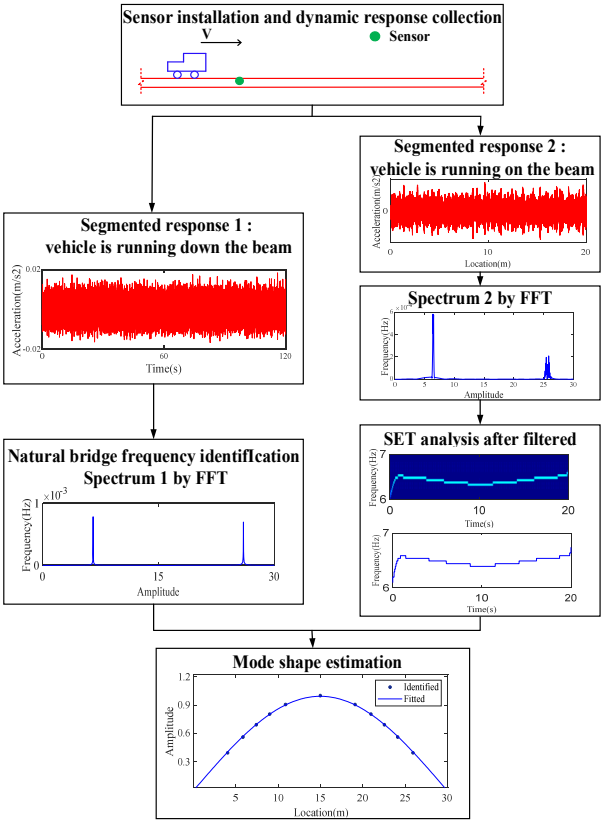

Fig. 3 Modal identification procedure

responses corresponding to each frequency of the bridge according to the range of the frequency peaks in the Spectrogram 2.

Step 4: Time-frequency ridge extraction. The SET is used to perform time-frequency analysis on the acceleration responses corresponding to each frequency of the moving VBS system separated in Step 3. The IF ridges of the moving VBS are obtained by the modulus maximum ridge extraction method, and the midpoints of the staircase curve in the IF ridge diagram are selected as the effective data points for IF calculation.

Step 5: Mode shape estimation. The bridge mode shape points are calculated by combining Eq. (13) and the effective data points selected in Step 4, and mode shapes are estimated through the least squares fitting method and the maximum normalization. The sign of the mode shape can be determined according to engineers' judgment or experience (Fang and Perera 2009).

The proposed method can reduce the number of sensors and the workload of data processing, and improve the mode shape accuracy by transforming the mode shape identification into frequency identification.

4. Numerical study

4.1 FEM of the moving VBS

A FEM for the moving VBS is developed and shown in Fig. 4. The bridge model consists of discretized Euler beam elements with 4 degrees of freedom (2 per node). The

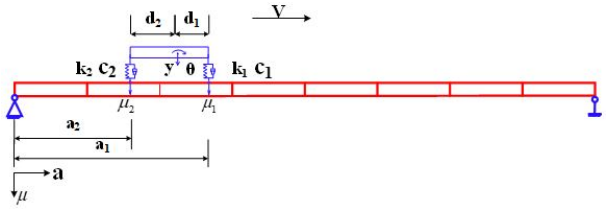

Fig. 4 FEM of the moving VBS

bridge has constant mass per unit length ρ, elastic modulus E and inertia moment I. The vehicle is simplified as a mass supported by two-axle springs with mass weight m_v, rotation stiffness j, and the velocity V. The lengths of the two axles from the center of gravity of the vehicle are d_1 and d_2, respectively.

The response of the vehicle is given by the system equations

$$m_v\ddot{y} + c_1(\dot{y} + d_1\dot{\theta} - \dot{\mu}_1) + c_2(\dot{y} - d_2\dot{\theta} - \dot{\mu}_2) + k_1(y + d_1\theta - \mu_1) + k_2(y - d_2\theta - \mu_2) = 0 \tag{23}$$

$$j\ddot{\theta} + c_1d_1(\dot{y} + d_1\dot{\theta} - \dot{\mu}_1) - c_2d_2(\dot{y} - d_2\dot{\theta} - \dot{\mu}_2) + k_1d_1(y + d_1\theta - \mu_1) - k_2d_2(y - d_2\theta - \mu_2) = 0 \tag{24}$$

in which μ_1 and μ_2 denote the vertical displacement of the front and rear axles of the vehicle at the contact positions of the bridge, respectively. y and θ denote the vertical displacement and angular displacement of the vehicle, respectively.

The combination of Eqs. (24)-(25) is written as

$$M_v\ddot{Y}_v + C_v\dot{Y}_v + K_vY_v = P_v \tag{25}$$

in which Y_v, M_v, C_v, K_v and P_v denote the displacement vector, mass matrix, damping matrix, stiffness matrix and external load vector of the vehicle, respectively.

$$Y_v^T = [y \quad \theta]$$
$$M_v = \begin{bmatrix} m_v & 0 \\ 0 & J_v \end{bmatrix}$$
$$C_v = \begin{bmatrix} c_1 + c_2 & c_1d_1 - c_2d_2 \\ c_1d_1 - c_2d_2 & c_1d_1^2 + c_2d_2^2 \end{bmatrix}$$
$$K_v = \begin{bmatrix} k_1 + k_2 & k_1d_1 - k_2d_2 \\ k_1d_1 - k_2d_2 & k_1d_1^2 + k_2d_2^2 \end{bmatrix}$$
$$P_v^T = \begin{bmatrix} c_1\dot{\mu}_1 + c_2\dot{\mu}_2 & c_1d_1\dot{\mu}_1 - c_2d_2\dot{\mu}_2 \\ +k_1\mu_1 + k_2\mu_2 & +k_1d_1\mu_1 - k_2d_2\mu_2 \end{bmatrix}$$

The motion equation of the bridge is

$$M_b\ddot{Y}_b + C_b\dot{Y}_b + K_bY_b = P_b \tag{26}$$

in which M_b and K_b denote the mass matrix and stiffness matrix of the bridge, respectively. C_b is the bridge damping matrix (Rayleigh damping model, $C_b = \varepsilon_0M_b + \varepsilon_1K_b$).

The external load vector P_b can be expressed as

$$P_b = N_1^Tf_1 + N_2^Tf_2 \tag{27}$$

The contact forces of the front and rear wheels at the contact positions are calculated as

$$f_1 = c_1(\dot{y} + d_1\dot{\theta} - \dot{\mu}_1) + k_1(y + d_1\theta - \mu_1) + \frac{d_2}{d_1 + d_2}m_vg \tag{28}$$

$$f_2 = c_2(\dot{y} - d_2\dot{\theta} - \dot{\mu}_2) + k_2(y - d_2\theta - \mu_2) + \frac{d_1}{d_1 + d_2}m_vg \tag{29}$$

The bridge vertical displacement is equal to the vertical displacement at the contact positions of the beam element and the wheel, which can be expressed by the shape function (N) and the degree-of-freedoms of the beam element as

$$\mu_i = N_i \cdot Y_b \tag{30}$$

$$\dot{\mu}_i = N_i \cdot \dot{Y}_b + N_{ia} \cdot V \cdot Y_b \tag{31}$$

in which N_{ia} is the first derivative of N_i to a.

Combining Eqs. (26)-(27), the motion equation of the moving VBS can be established as

$$\begin{bmatrix} M_b & 0 & 0 \\ 0 & & \\ 0 & M_v & \end{bmatrix}\begin{Bmatrix} \ddot{Y}_b \\ \ddot{y} \\ \ddot{\theta} \end{Bmatrix} + \begin{bmatrix} C_z & -c_1N_1^T - c_2N_2^T & -c_1d_1N_1^T - c_2d_2N_2^T \\ -c_1N_1 - c_2N_2 & & \\ -c_1d_1N_1 + c_2d_2N_2 & C_v & \end{bmatrix}\begin{Bmatrix} \dot{Y}_b \\ \dot{y} \\ \dot{\theta} \end{Bmatrix} + \begin{bmatrix} K_z & -k_1N_1^T - k_2N_2^T & -k_1d_1N_1^T + k_2d_2N_2^T \\ -k_1N_1 - k_2N_2 - c_1VN_{1a} - c_2VN_{2a} & & \\ -k_1d_1N_1 + k_2d_2N_2 + c_1d_1VN_{1a} + c_2d_2VN_{2a} & K_v & \end{bmatrix}\begin{Bmatrix} Y_b \\ y \\ \theta \end{Bmatrix} = \begin{bmatrix} P_z \\ 0 \\ 0 \end{bmatrix} \tag{32}$$

in which C_z, K_z and P_z can be calculated as

$$C_z = C_b + c_1 \cdot N_1^TN_1 + c_2 \cdot N_2^TN_2$$
$$K_z = K_b + k_1N_1^TN_1 + k_2N_2^TN_2 + c_1 \cdot V \cdot N_1^TN_{1a} + c_2 \cdot V \cdot N_2^TN_{2a}$$
$$\boldsymbol{P_z = N_1^T\frac{d_2}{d_1 + d_2}m_vg + N_2^T\frac{d_1}{d_1 + d_2}m_vg}$$

4.2 Modal identification

A simply supported beam and a two-span continuous beam with equal cross-section are simulated to verify the feasibility and effectiveness of the proposed modal identification method. The parameters of the simply supported beam are the same as those utilized in Ref. Yang *et al.* (2019). As shown in Fig. 4, the simply supported beam has length of $30\,m$, cross-sectional area of $1.8\,m^2$, inertia moment of $0.2\,m^4$, mass per unit length of $2000\,kg/m^3$, and elastic modulus of $27.5\,GPa$. The first two natural frequencies of the beam are $2.89\,Hz$ and

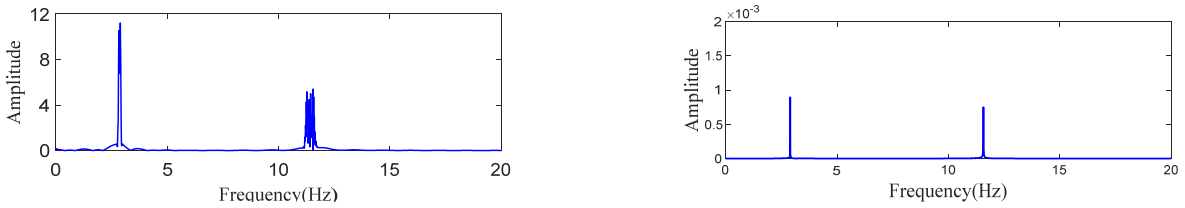

(a) The vehicle is running on the beam (b)The vehicle is running down the beam

Fig. 5 Acceleration spectrum of the simply supported beam

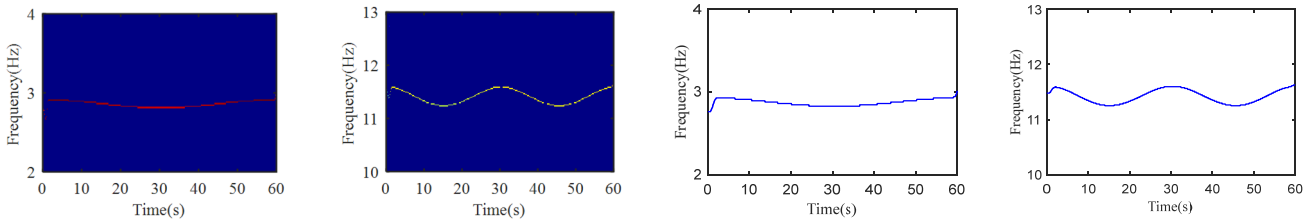

(a) TF diagram (b) IF ridge diagram

Fig. 6 Extracted instantaneous frequency of the simply supported beam

$11.58\,Hz$, respectively. The beam is modeled by Euler beam elements with the length of $1\,m$. The main parameters of the two-axle asymmetric vehicle are: vehicle weight $m_v = 1800\,kg$, wheel base $d_1 = d_2 = 0.2\,m$, stiffness $k_1 = k_2 = 1.2 \times 10^5\,kN/m$, and mass moment of inertia relative to the mass center $j = 2300\,kg \cdot m^2$. The vehicle velocity and the time step of the dynamic analysis are set to be $0.5\,m/s$ and $0.001\,s$, respectively. An acceleration sensor is assumed to be installed at one-third of the span. Considering the fact that only low modes can be excited for girder bridges in field, only the first two mode shapes are identified in this example. The frequencies and modes shapes are then identified following the procedures presented in Section 3.2.

The measured acceleration response is divided into two parts, i.e., the moving VBS dynamic response when the vehicle is running on the beam and the simply-supported beam dynamic response after the vehicle running down the beam. FFT is employed to analyze the two response parts and the results are plotted in Fig. 5. The first two frequencies of the simply-supported beam can be identified as $2.91\,Hz$ and $11.61\,Hz$ through Fig. 5(b), respectively, which are in continent with the references results calculated by densely meshed FEM ($2.89\,Hz$ and $11.58\,Hz$). Distinct differences can be found between the spectrograms when the vehicle is running on the beam and after the vehicle running down the beam due to the mass property of the vehicle. As shown in Fig. 5(a), multiple peaks appear in the system acceleration spectrogram when the vehicle is running on the beam, which indicates that each frequency of the system changes within a certain range caused due to the movement of the vehicle.

The acceleration responses corresponding to the first two frequencies of the beam are separated according to the range of the frequency peaks in the spectrogram by the band-pass filter. Fig. 6(a) shows the time-frequency diagram of the system obtained by the SET, and Fig. 6(b) presents the corresponding time-frequency ridge obtained by the modulus maximum ridge extraction method. The 13 midpoints of the first-order staircase curve and 86 midpoints of the second-order staircase curve in Fig. 6(b) are selected as the effective data points for IF calculation. The mode shapes are then calculated via Eq. (13) and least squares fitting method. Fig. 7 compares the identified and reference mode shapes. Modal assurance criterion (MAC) is used to quantify the matching degree between the identified and reference mode shapes (Gres *et al.* 2021). The MAC values are not listed as they are all larger than 0.9990. The results clearly demonstrate that the proposed method can identify the modal parameters of the simply supported beam with high accuracy.

The proposed identification method is further performed on the two-span continuous beam. An acceleration sensor is assumed to be installed at one-third of the left span. The length of each span is $15\,m$, the elastic modulus is $22.5\,Gpa$, and other parameters of the bridge and vehicle are the same as the simply-supported beam example. The first two frequencies of the two-span continuous beam can be identified as $10.47\,Hz$ and $16.02\,Hz$ through FFT results, respectively, which are in continent with the references results calculated by densely meshed FEM ($10.47\,Hz$ and $16.36\,Hz$). Fig. 8 presents the identified and referenced mode shapes of the two-span continuous beam. The results manifest that the proposed modal identification method is still valid for the continuous beam with one sensor.

4.3 Discussion

This section discusses the influence of various factors including vehicle weight, vehicle velocity, wheel base, and measurement positions on the identification accuracy of the proposed method. The scenarios of different vehicle parameters considered in this section are listed in Table 1. The identification procedures are the same as in Section 3.2 and are not illustrated in detail in this section. The first two

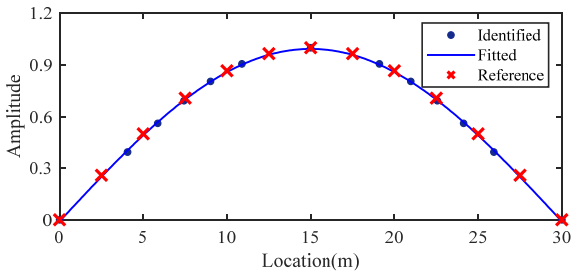

(a) The first mode shape

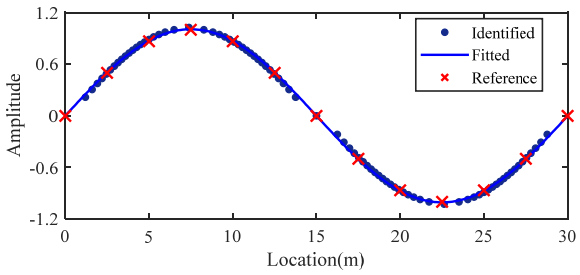

(b) The second mode shape

Fig. 7 Mode shape identification results of the simply supported beam

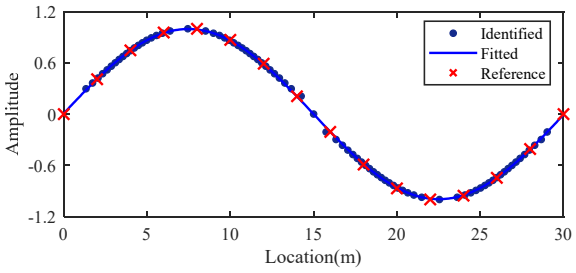

(a) The first mode shape

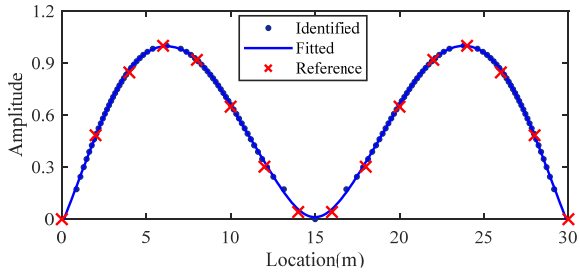

(b) The second mode shape

Fig. 7 Mode shape identification results of the continuous beam

Table 1 Vehicle parameters and the MAC results of different scenarios

Factors	Scenario	m_v (kg)	d_1 (m)	d_2 (m)	V (m/s)	MAC-1*	MAC-2
Vehicle weight	Case VW1	1000	0.2	0.2	0.5	0.9961	0.9980
	Case VW2	2000	0.2	0.2	0.5	0.9977	0.9994
	Case VW3	3000	0.2	0.2	0.5	0.9999	0.9995
Vehicle velocity	Case VV1	1800	0.2	0.2	1	0.9996	0.9995
	Case VV2	1800	0.2	0.2	2	0.9994	0.9984
	Case VV3	1800	0.2	0.2	3	0.9875	0.9983
Wheel base	Case WB1	3000	0.2	0.2	1	0.9988	0.9992
	Case WB2	3000	0.4	0.4	1	/	0.9965
	Case WB3	3000	1	0.6	1	0.9818	0.9921

*MAC-1: first mode shape; MAC-2: second mode shape

frequencies are identified as $2.91\,Hz$ and $11.61\,Hz$ in all scenarios as the frequencies are identified via the dynamic response of the beam after the vehicle running down the beam which is irrelevant to the vehicle. Therefore, only the influence on the identification accuracy of mode shapes will be discussed.

4.3.1 Vehicle weight

Considering the fact that the mass ratio of vehicle to beam in the field of civil engineering is usually less than 5%, three vehicle weights, specific as $1000\,kg$, $2000\,kg$ and $3000\,kg$ (the mass ratios are 1.7%, 3.3% and 5%) are used herein for parametric study. The identified mode shapes are plotted in Figs. 9-11. The energy of the time-frequency diagram of the system for SET becomes more concentrated and the effective data points on the time-frequency ridge curve increase with the vehicle weight, which results in the increasing accuracy of the mode shape identification. As shown in Figs. 9-11, the identified first mode shapes have 7, 15 and 18 effective data points when the vehicle weight is $1000\,kg$, $2000\,kg$ and $3000\,kg$, respectively. The increase of effective data points makes the fitting mode curve smoother and more accurate. Table 1 lists the MAC values between the identified mode shapes and referenced ones, which verify that the proposed method can identify the mode shapes with enough accuracy under different vehicle weights. Within the range of the common mass ratio of vehicle to bridge, larger vehicle weight will bring higher identification accuracy.

4.3.2 Vehicle velocity

Three vehicle velocities, specific as $1\,m/s$, $2\,m/s$, and $3\,m/s$ are simulated to investigate the vehicle velocity effects. The vehicle weight is set to be $3000k\,g$, and other

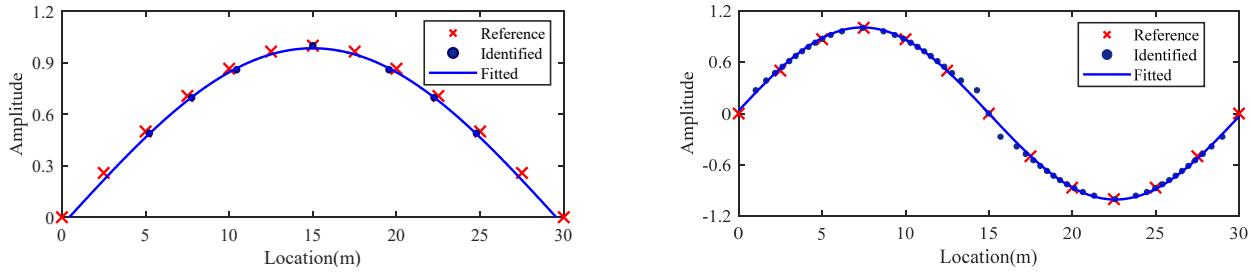

(a) The first mode shape (b) The second mode shape

Fig. 9 Mode shape identification results of Case VW1

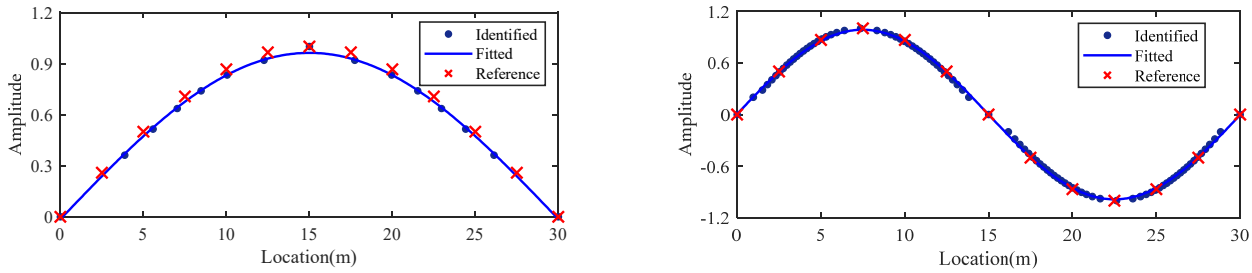

(a) The first mode shape (b) The second mode shape

Fig. 10 Mode shape identification results of Case VW2

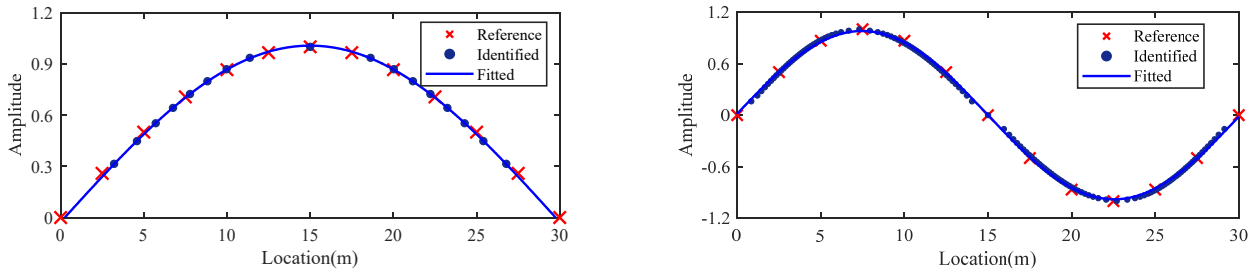

(a) The first mode shape (b) The second mode shape

Fig. 11 Mode shape identification results of Case VW3

parameters stay the same with Section 3.2. The MAC values as listed in Table 1 manifest that the mode shape identification accuracy decreases with the vehicle velocity. This is because a higher velocity will shorten the moving time of the vehicle on the bridge and reduce the effective data points obtained by the SET of time-frequency analysis. When the velocity is too high (more than 3 m/s), the proposed method can hardly identify the first mode shape due to very limited effective data points.

4.3.3 Wheel base

Three wheel bases, specific as 0.2 m, 0.4 m and 0.6 m are simulated to investigate the vehicle wheel base effects, which are deemed as cases WB1, WB2 and WB3, respectively. The vehicle velocity is set to be 1m/s, the weight is $3000\ kg$ and other parameters are the same as in Section 3.2. As shown in Table 1, the mode shape identification accuracy increases with the wheelbase. The proposed method is efficient when the ration of the vehicle length to bridge length is less than 4%. However, the SET cannot calculate the time-frequency of the IF of the VBI system for Case WB2 (Fig. 12) as the vehicle frequency approaches to the bridge frequency, and thus the mode shapes cannot be identified.

4.3.4 Measurement position

Vertical accelerations collected at three positions, i.e., 1/2, 1/4 and 2/3 of the span from the left support, are analyzed to study the effect of measurement positions. The extracted mode shapes from the responses measured at different positions are presented in Fig. 13. When the sensor is installed at the mid-span of a simply supported beam, the even-order modal parameters cannot be identified. The results obtained from the sensors installed at other positions agree well with each other.

The results of the simulated simply supported beam and continuous beam verify that the proposed method can identify the modal parameters with high accuracy at the cost of single sensor. The discussions on the effects of different factors verify the effectiveness and superiority of the proposed method under different environments.

Fig. 12 The TF diagram of Case WB3

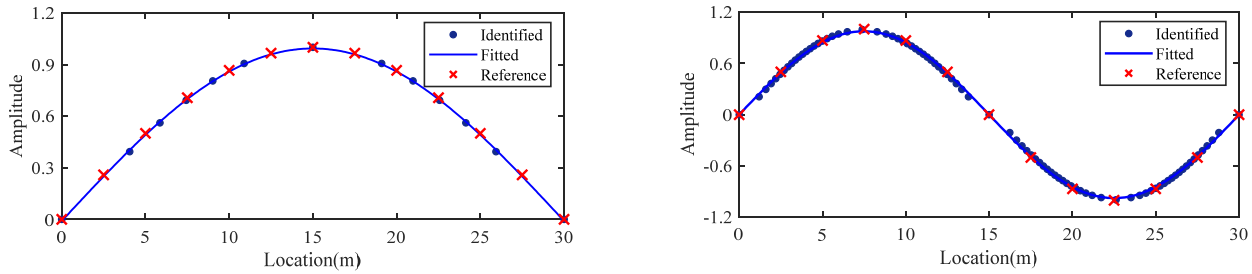

(a) The first mode shape (b) The second mode shape

Fig. 13 Mode shape identification results of different measurement positions

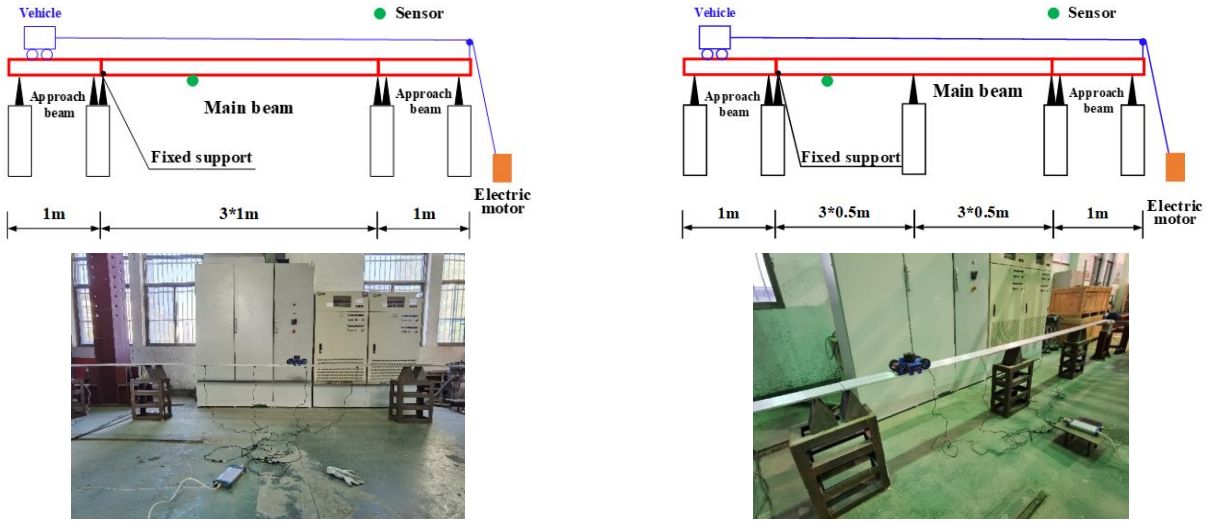

(a) The simply supported beam (b) The continuous beam

Fig. 14 Arrangement and configuration of the experimental beam

A simply supported aluminum beam and a continuous aluminum beam are employed to examine the feasibility and effectiveness of the proposed method in the laboratory environment (Fig. 14). The simply supported beam has length of $3\,m$, section height of $25\,mm$ and section thickness of $125\,mm$. The continuous beam has length of $3\,m$, section height of $10\,mm$ and section thickness of $130\,mm$. Two aluminum beams with a length of $1m$ are placed at both ends of the main beam to ensure that the vehicle reaching the preset velocity, moving stability on the main beam, and decelerating smoothly after exiting the main beam. The axle distances of the test vehicle are $d_1 = d_2 = 0.075\,m$, and the weight is $m_v = 0.5\,kg$. The total weight of the vehicle can be changed by adjusting the number of additional weights placed on the vehicle. A sensor is installed on one-third of the span of the beam.

5. Experimental study

Four sets of experiments were carried out on the simply supported beam and continuous as listed in Table 2. Only the responses corresponding to the first-order modal parameters are selected for modal identification. To save space, Experimental S3 and Experiment C2 are employed to illustrate the performance of the proposed method. The first-order frequencies of simply supported beam and continuous beam are identified as $6.81\,Hz$ and $10.23\,Hz$,

Table 2 Test vehicle parameters

Simply supported beam	Continuous beam	$m_v(kg)$	$V(m/s)$
Experiment S1	Experiment C1	2.5	0.15
Experiment S2	Experiment C2	2.5	0.3
Experiment S3	Experiment C3	3.5	0.6
Experiment S4	Experiment C4	4.5	0.6

Table 3 The updating coefficients

Experiment	e_1	e_2	e_3	e_4
Experiment S3	1.0000	1.0412	0.9772	1.0222
Experiment C2	1.0000	0.9979	1.0010	0.9999

respectively. The corresponding mode shapes are plotted in Fig. 15. The MAC values of Experiments S3 and C2 are 0.9988 and 0.9923. Similar results are obtained for other scenarios, which demonstrate that the proposed method can obtain the mode shapes with high-precision at the cost of only single sensor under the experimental environment.

6. Application in FEM updating

The establishment of a reliable FEM is the foundation for bridge dynamic analysis and safety assessment. However, the initial FEM established according to the design drawing is normally different from the real structure due to the simplification of boundary condition, deviation of material and geometry parameter and so on (Razavi and Hadidi 2020, Alpaslan and Karaca 2021). Therefore, it is essential to update the initial FEM to make the measured modal parameters approximate to the modal parameters calculated by the FEM as much as possible (Ni *et al*. 2012, Ho *et al*. 2020, Friswell and Mottershead 2013). In order to verify the applicability of the proposed method, the initial FEMs are updated using the identified modal parameters in Section 5. The FEM updating mainly includes three key issues, namely, the selection of updating parameters, the determination of the objective function and the optimization

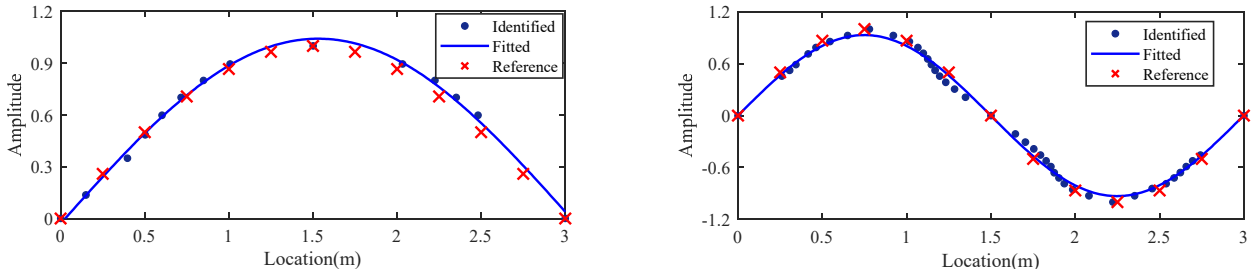

(a) Experiment S3 (b) Experiment C2

Fig. 15 Experimental mode shape results

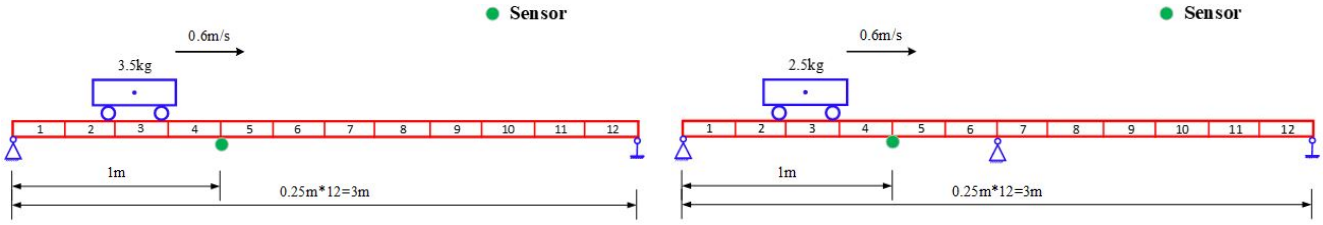

(a) The simply supported beam (b) The continuous beam

Fig. 16 The initial FEM of the experimental beams

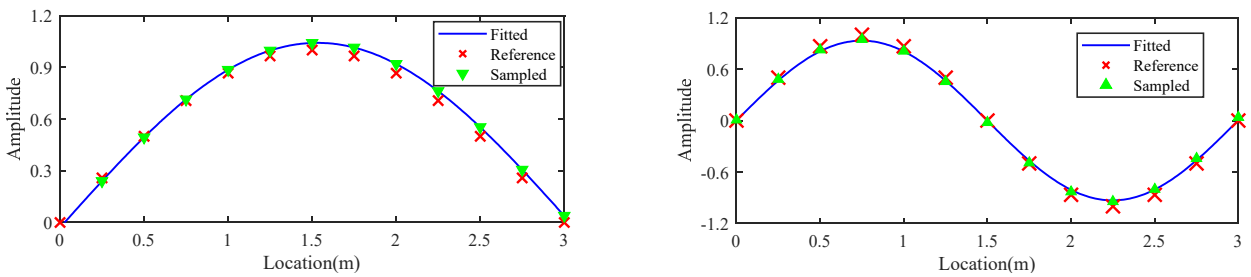

(a) The simply supported beam (b) The continuous beam

Fig. 17 Experimental mode shape sampling

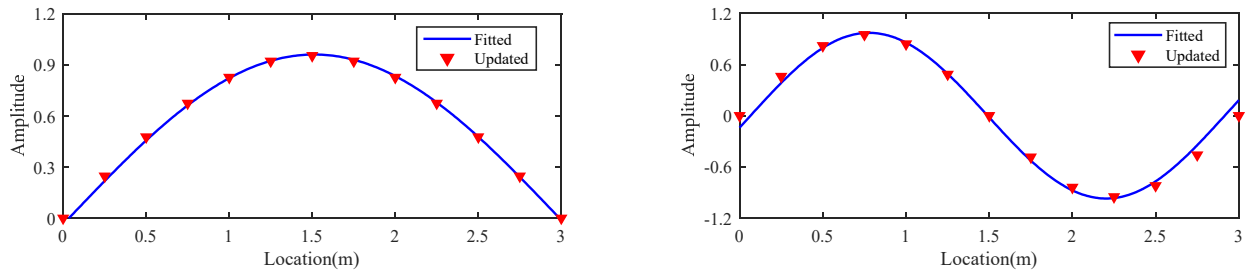

(a) S3 (b) C2

Fig. 18 Mode shapes after FEM updating

Table 4 Frequency and MAC comparison before and after updating

Case	Measured	Initial FEM			Updated FEM		
	Frequency (Hz)	Frequency (Hz)	Relative error (%)	MAC	Frequency (Hz)	Relative error (%)	MAC
Experiment S3	6.83	6.41	6.15	0.9988	6.83	0.00	0.9998
Experiment C2	10.23	10.27	0.39	0.9923	10.24	0.09	0.9981

algorithm (Ho *et al*. 2019).

As shown in Fig. 16, the initial FEM parameters of beams are the same as those in Section 5. The beam elastic modulus E, section height h, section width b and mass per linear meter ρ are selected as updating parameters. The objective function $Q(\boldsymbol{p})$ is formulated via the commonly used frequency and MAC as

$$\lambda_{ti} = (2\pi w_{ti})^2 \tag{33}$$

$$\lambda_{ei} = (2\pi w_{ei})^2 \tag{34}$$

$$MAC_i = \frac{(\phi_{ti}^T \phi_{ei})^2}{(\phi_{ti}^T \phi_{ti})(\phi_{ei}^T \phi_{ei})} \tag{35}$$

$$Q(\boldsymbol{p}) = \sum_{i=1}^{n} \chi_i \left[\frac{\lambda_{ti}(\boldsymbol{p}) - \lambda_{ei}}{\lambda_{ei}}\right]^2 + \sum_{i=1}^{n} \beta_i \left[sqrt(MAC_i) - 1\right]^2 \quad \text{(i=1,2)} \tag{36}$$

where the vector $\boldsymbol{p} = [E, h, b, \rho] \in R^n$ represents the parameter set to be updated; w_{ti} and ϕ_{ti} represent the i^{th} frequency and mode shapes calculated by the FEM; w_{ei} and ϕ_{ei} represent the i^{th} frequency and mode shapes identified by the experimental data. χ_i and β_i are the weight coefficients, generally determined according to the importance and measurement accuracy, and they are set to be unit in this study.

The sequential quadratic programming method (Gill *et al*. 2005) is selected as the optimization algorithm to obtain the updating coefficients defined as the ratios of the updating parameters to the initial parameters. The updating coefficients of the section width b, section height h, mass per linear meter ρ and the bridge elastic modulus $E$are deemed as e_1, e_2, e_3 and e_4, respectively.

As shown in Fig. 17, 13 modal points are sampled equidistantly on the mode fitting curve of Experiment S3 and Experiment C2 according to the node positions, respectively. The initial FEMs of the simply supported beam and continuous beam are updated using the first two frequencies and MACs identified in Section 5, and the results of the updating coefficients are listed in Table 3. The comparison of frequency and MAC values before and after updating are displayed in Table 4. The mode shapes of Experiments S3 and C2 are compared in Fig. 18. After updating, the modal parameters calculated by the FEMs are consistent with the measured results. For example, the relative error of the first frequency of the simply supported beam decreases from 6.15% to 0.00%. The experiments proved that the modal parameters identified by the proposed method can provide reliable data for FEM updating.

7. Conclusions

This paper proposed a modal identification method of time-varying VBS using a single sensor. Firstly, the physical relationship between the IF of the VBS and the bridge mode shape was deduced. Then the bridge modal identification method based on the IF tracking of the VBS was proposed in which the mode shape identification was transformed into system frequency identification. Numerical studies and laboratory experiments of simply supported beam and continuous beam verified that the proposed method could identify modal parameters effectively at the cost of a single sensor. The influence of vehicle weight, vehicle velocity, wheel base and the measurement position were studied systematically through numerical studies. The results demonstrated that the greater the vehicle weight, the lower the velocity, and the smaller the wheel base led to higher identification accuracy within the common vehicle-to-bridge mass ratio range, the measurement position didn't affect the identification accuracy except for the middle span. Finally, the modal

parameters identified by the proposed method were applied successfully in FEM updating. However, the actual feasibility of the proposed method should be further verified through real bridge experiments in the future. Besides, the identification of damping ratio needs further study, which is also one of important works of modal identification.

Acknowledgments

The paper is supported by the National Natural Science Foundation of China (No. 51878234, 51778550 and 51778204), Natural Science Fund for Distinguished Young Scholars of Anhui Province (2208085J20) , Fundamental Research Funds for the Central Universities (No. JZ2019HGPA0101), Shenzhen Science and Technology Program (No. KQTD20180412181337494), Scientific Research Fund of Hunan Provincial Education Department (Project No. 19B106), Natural Science Foundation of Hunan Province Province (No. 2021JJ50145).

References

Alpaslan, E. and Karaca, Z. (2021), "Response surface-based model updating to detect damage on reduced-scale masonry arch bridge", *Struct. Eng. Mech., Int. J.*, **79**(1), 9-22. https://doi.org/10.12989/sem.2021.79.1.009

Babakhani, B., Rahami, H. and Mohammadi, R.K. (2018), "Mode shape identification using response spectrum in experimental modal analysis", *Struct. Monit. Maint., Int. J.*, **5**(3), 345-361. https://doi.org/10.12989/smm.2018.5.3.345

Boashash, B. and Aïssa-El-Bey, A. (2018), "Robust multisensor time–frequency signal processing: A tutorial review with illustrations of performance enhancement in selected application areas", *Digit Signal Process*, **77**, 153-186. https://doi.org/10.1016/j.dsp.2017.11.017

Chang, M., Kim, J.K. and Lee, J. (2019), "Hierarchical neural network for damage detection using modal parameters", *Struct. Eng. Mech., Int. J.*, **70**(4), 457-466. https://doi.org/10.12989/sem.2019.70.4.457

Fang, S.E. and Perera, R. (2009), "Power mode shapes for early damage detection in linear structures", *J. Sound Vib.*, **324**(1-2), 40-56. https://doi.org/10.1016/j.jsv.2009.02.002

Friswell, M. and Mottershead, J.E. (2013), *Finite Element Model Updating in Structural Dynamics*, Springer Science & Business Media, London, UK.

Frýba, L. (1996), *Dynamics of Railway Bridges*, Thomas Telford Publishing, London, UK.

Gill, P.E., Muttay, W. and Saunders, M.A. (2005), "SNOPT: An SQP algorithm for large-scale constrained optimization", *SIAM Rev. Soc. Ind. Appl. Math.*, **47**(1), 99-131. https://doi.org/10.1137/S1052623499350013

González, A., Obrien, E.J. and McGetrick, P.J. (2012), "Identification of damping in a bridge using a moving instrumented vehicle", *J. Sound Vib.*, **331**(18), 4115-4131. https://doi.org/10.1016/j.jsv.2012.04.019

Gres, S., Dohler, M. and Mevel, L. (2021), "Uncertainty quantification of the Modal Assurance Criterion in operational modal analysis", *Mech. Syst. Signal Process.*, **152**, 107457. https://doi.org/10.1016/j.ymssp.2020.107457

He, W.Y., Ren, W.X. and Zuo, X.H. (2018), "Mass-normalized mode shape identification method for bridge structures using parking vehicle-induced frequency change", *Struct. Control Health Monitor.*, **25**(6), e2174. https://doi.org/10.1002/stc.2174

Ho, L.V., Khatir, S., Roeck, G.D. and Bui-Tien, T. (2020), "Finite element model updating of a cable-stayed bridge using metaheuristic algorithms combined with Morris method for sensitivity analysis", *Smart Struct. Syst., Int. J.*, **26**(4), 451-468. https://doi.org/10.12989/sss.2020.26.4.451

Kim, C.W. and Kawatani, M. (2008), "Pseudo-static approach for damage identification of bridges based on coupling vibration with a moving vehicle", *Struct. Infrastruct. Eng.*, **4**(5), 371-379. https://doi.org/10.1080/15732470701270082

Kim, C.Y., Jung, D.S., Kim, N.S., Kwon, S.D. and Feng, M.Q. (2003), "Effect of vehicle weight on natural frequencies of bridges measured from traffic-induced vibration", *Earthq. Eng. Eng. Vib.*, **2**(1), 109-115. https://doi.org/10.1007/bf02857543

Kong, X., Cai, C.S. and Kong, B. (2016), "Numerically extracting bridge modal properties from dynamic responses of moving vehicles", *J. Eng. Mech.*, **142**(6), 04016025. https://doi.org/10.1061/(ASCE)EM.1943-7889.0001033

Li, J.T., Zhu, X.Q., Law, S.S. and Samali, B. (2020), "Time-varying characteristics of bridges under the passage of vehicles using synchroextracting transform", *Mech. Syst. Signal Process.*, **140**, 106727. https://doi.org/10.1016/j.ymssp.2020.106727

Magrab, E.B. (2012), *Vibrations of Elastic Systems: With Applications to MEMS And NEMS*, Springer Science & Business Media, London, UK.

Mahato, S., Hazra, B. and Chakraborty, A. (2020), "Multi-variate empirical mode decomposition (memd) for ambient modal identification of rc road bridge", *Struct. Monitor. Maint., Int. J.*, **7**(4), 283-294. https://doi.org/10.12989/smm.2020.7.4.283

Meignen, S., Oberlin, T., Depalle, P., Flandrin, P. and McLaughlin, S. (2016), "Adaptive multimode signal reconstruction from time–frequency representations", *Philos. Trans. A Math. Phys. Eng. Sci.*, **374**(2065), 20150205. https://doi.org/10.1098/rsta.2015.0205

Ni, Y.Q., Xia, Y., Lin, W., Chen, W.H. and Ko, J.M. (2012), "SHM benchmark for high-rise structures: a reduced-order finite element model and field measurement data", *Smart Struct. Syst., Int. J.*, **10**(4-5), 411-426. https://doi.org/10.12989/sss.2012.10.4_5.411

Ni, P.H., Li, J., Hao, H., Xia, Y., Wang, X.Y., Lee, J.M., Jung, K.H. (2018), "Time-varying System Identification using Variational Mode Decomposition", *Struct. Control Health Monitor.*, **25**(6), e2175. https://doi.org/10.1002/stc.2175

Oberlin, T., Meignen, S. and Perrier, V. (2015), "Second-order synchrosqueezing transform or invertible reassignment? Towards ideal time-frequency representations", *IEEE Trans. Signal Process.*, **63**(5), 1335-1344. https://doi.org/10.1109/TSP.2015.2391077

Obrien, E.J. and Malekjafarian, A. (2016), "A mode shape-based damage detection approach using laser measurement from a vehicle crossing a simply supported bridge", *Struct. Control Health Monitor.*, **23**(10), 1273-1286. https://doi.org/10.1002/stc.1841

Razavi, M. and Hadidi, A. (2020), "Assessment of sensitivity-based FE model updating technique for damage detection in large space structures", *Struct. Monitor. Maint., Int. J.*, **7**(3), 261-281. https://doi.org/10.12989/smm.2020.7.3.261

Ribeiroa, D., Calçadab, R., Delgadob, R., Brehmc, M. and Zabeld, V. (2012), "Finite element model updating of a bowstring-arch railway bridge based on experimental modal parameters", *Eng. Struct.*, **40**, 413-435. https://doi.org/10.1016/j.engstruct.2012.03.013

Tran, N.H., Khatir, S., De Roeck, G., Long, N.N., Thanh, B.T. and Wahab, M.A. (2020), "An efficient approach for model updating of a large-scale cable-stayed bridge using ambient vibration measurements combined with a hybrid metaheuristic search

algorithm", *Smart Struct. Syst., Int. J.*, **25**(4), 487-499. https://doi.org/10.12989/sss.2020.25.4.487

Xin, Y., Hao, H. and Li, J. (2019), "Time-varying system identification by enhanced Empirical Wavelet Transform based on Synchroextracting Transform", *Eng. Struct.*, **196**, 109313. https://doi.org/10.1016/j.engstruct.2019.109313

Yang, Y.B. and Lin, C.W. (2005), "Vehicle-bridge interaction dynamics and potential applications", *J. Sound Vib.*, **284**(1-2), 205-226. https://doi.org/10.1016/j.jsv.2004.06.032.

Yang, Y.B., Lin, C.W. and Yau, J.D. (2004), "Extracting bridge frequencies from the dynamic response of a passing vehicle", *J. Sound Vib.*, **272**(3-5), 471-493. https://doi.org/10.1016/S0022-460X(03)00378-X

Yang, Y.B., Li, Y.C. and Chang, K.C. (2012), "Effect of road surface roughness on the response of a moving vehicle for identification of bridge frequencies", *Inter. Mult. Mech.*, **5**(4), 347-368. https://doi.org/10.12989/imm.2012.5.4.347

Yang, Y.B., Cheng, M.C. and Chang, K.C. (2013), "Frequency variation in vehicle–bridge interaction systems", *Int. J. Struct. Stab. Dyn.*, **13**(2), 1350019. https://doi.org/10.1142/S02194554 13500193

Yang, Y.B., Zhang, B., Wang, T.Y., Xu, H. and Wu, Y.T. (2019), "Two-axle test vehicle for bridges: theory and applications", *Int. J. Mech. Sci.*, **152**, 51-62. https://doi.org/10.1016/j.ijmecsci.2018.12.043

Yu G., Yu, M.J. and Xu, C.Y. (2017), "Synchroextracting transform", *IEEE Trans. Ind. Electron.*, **64**(10), 8042-8054. https://doi.org/10.1109/TIE.2017.2696503

Yuan, P.P., Cheng, X.L., Wang, H.H., Zhang, J., Shen, Z.X. and Ren, W.X. (2021), "Structural instantaneous frequency extraction based on improved multi-synchrosqueezing generalized S-transform", *Smart Struct. Syst., Int. J.*, **28**(5), 675-687. https://doi.org/10.12989/sss.2021.28.5.675

Zhang, Y., Zhao, H.S. and Lie, S.T. (2019), "Estimation of mode shapes of beam-like structures by a moving lumped mass", *Eng. Struct.*, **180**, 654-668. https://doi.org/10.1016/j.engstruct.2018. 11.074

Zhang, J., Yang, D., Ren, W.X. and Yuan, Y. (2021), "Time-varying characteristics analysis of vehicle-bridge interaction system based on modified S-transform reassignment technique", *Mech. Syst. Signal Process.*, **160**, 107807. https://doi.org/10.1016/j.ymssp.2021.107807

Zhang, Y.M., Wang, H, Bai, Y., Mao, J.X. and Xu, Y.C. (2022), "Bayesian dynamic regression for reconstructing missing data in structural health monitoring", *Struct. Health Monitor.*, 14759217211053779. https://doi.org/10.1177/14759217211053779